RSC Advances

PAPER

View Article Online
View Journal | View Issue

Cite this: *RSC Adv.*, 2021, **11**, 23901

Electrospinning preparation and anti-infrared radiation performance of silica/titanium dioxide composite nanofiber membrane

Yilong Song,[a] Fang Zhao,*[a] Zhizun Li,[a] Zhaogang Cheng,[a] Hongjun Huang[a] and Mifen Yang[b]

Received 19th May 2021
Accepted 30th June 2021

DOI: 10.1039/d1ra03917b

rsc.li/rsc-advances

Silica/titanium dioxide (SiO_2/TiO_2) composite nanofiber membranes with different TiO_2 content were prepared with the technology of electrospinning using ethyl orthosilicate, butyl titanate and polyvinyl pyrrolidone as silicon titanium sources and spinning aids. TGA, XRD, SEM and FT-IR were used to analyze the thermal decomposition process, phase composition, microscopic morphology and infrared properties of the products. The study showed that with the increase of the calcination temperature, the TiO_2 phase gradually changed from amorphous to anatase structure. Above 900 °C, a sample containing rutile TiO_2 with a higher refractive index was obtained. Simultaneously, the continuity of the sample deteriorated, and the mechanical properties deteriorated. The study found that after calcination at 900 °C, the fiber membrane with a TiO_2 content of 12% had the lowest cost and the best overall performance, with tensile strength being 3.09 MPa, and thermal conductivity at 500 °C being 0.0899 W m^{-1} K^{-1}, which is 20% lower than that of pure SiO_2 fiber membrane. This research provides a reference for the development of high temperature insulation materials with good flexibility.

Introduction

With the increasingly serious environmental problems worldwide, reducing energy consumption and greenhouse gas emissions, and achieving "carbon neutrality" as soon as possible, has become the consensus of most countries.[1] To achieve this goal, people use high-performance insulation materials in various fields. SiO_2 nanofiber membrane is considered to be a very promising high-efficiency heat insulation material due to its characteristics of high temperature resistance, corrosion resistance, heat insulation performance at normal temperature, and good flexibility.[2] According to Stefan–Boltzmann's law and Planck's law, in high temperature environments, near-infrared radiation is the main method of heat transfer among objects. However, pure SiO_2 is almost completely transparent to near-infrared radiation of 1–8 μm wavelength.[3,4] Therefore, improving the anti-infrared radiation ability of SiO_2 nanofiber membrane is key to extending its application prospects.

According to the energy band theory and the Fresnel formula, the anti-infrared radiation performance of a material is mainly related to its refractive index and band gap. Choosing an infrared opacifier with a high refractive index and a specific band gap, and doping a high-reflective coating on the fiber surface or doping a sunscreen phase in the fiber are the main measures to improve the infrared radiation resistance of fiber materials.[5] Titanium dioxide (TiO_2) is a typical broadband-absorbing semiconductor material with three crystal types, namely rutile, anatase and brookite. With a refractive index of 2.7, rutile TiO_2 is an inorganic oxide with higher refractive index.[6] Compared with traditional infrared-shading materials such as SiC and carbon black, TiO_2 has become an ideal infrared-shading agent for having stabler properties. Yang *et al.*[7] used the layer-by-layer (LBL) assembling technique to assemble nano-TiO_2 on the surface of PVDF fiber as insulations, and analyzed the influence of TiO_2 loading levels on the radiation-induced thermal conductivity. Results show that when the TiO_2 content was 5.7%, the radiation-induced thermal conductivity was reduced by nearly 43%. Utilizing hydrothermal growth, Ma *et al.*[8] cast a layer of TiO_2 coating on the surface of ZrO_2 fiber thus improving the fiber's mechanical strength and resistance to infrared radiation.

Existing reports have shown that TiO_2 helps reduce the infrared transmittance of fiber materials, but it has some shortcomings. On the one hand, the process of preparing the coating on the surface of the nanofiber is complicated and it is hard to ensure uniform coating. On the other, the TiO_2 film with high permittivity is easy to form a thermal bridge between the fibers, thereby greatly improving the thermal conductivity of the fibers at room temperature.[9] Although the fibers prepared by Ma *et al.* show reflective abilities for infrared waves, because the

[a]*Department of Vehicle and Electrical Engineering, Shijiazhuang Campus, Army Engineering University, Shijiazhuang 050003, China. E-mail: zhaofang19821106@163.com*

[b]*Basic Department, Shijiazhuang Campus, Army Engineering University, Shijiazhuang 050003, China*

TiO_2 coating caused the fibers to contact each other and forms a thermal bridge in the sample, the thermal conductivity of the ZrO_2 fibers coated with TiO_2 is as high as 0.6 W m^{-1} K^{-1}, which is 2.5 times that of pristine ZrO_2 fibers.[8] "Opacified Fibrous Insulations" proposed by Grunert *et al.* provides a theoretical basis for solving the above problems. The research pointed out that randomly distributing some reflective metallic particles or flakes in the fiber insulation material can effectively reduce the radiative heat transfer of the material.[10] Based on this theory, David *et al.*[11] incorporated TiO_2 particles into textiles and studied the radiative heat transfer characteristics of modified fabrics. Results show that the modified fabric had lower infrared transmittance compared with the fabric without doped particles. However, this method is limited in improving the fiber's ability to resist infrared radiation, because too high a particle content will worsen its dispersibility, and also destroy the continuity of the fiber. However, Zhao *et al.* found that adding ceramic particles to the spun fiber has limited changes in the infrared characteristics of the fiber. When the content of ceramic particles exceeds 8%, many properties of the fiber will be adversely affected, and its spinnability will become worse and the continuity will decrease.[12] Therefore, to develop anti-infrared radiation fiber membranes with excellent comprehensive performance, it is necessary to study many factors such as spinning solution and preparation technology.

In this work, we prepared SiO_2/TiO_2 composite nanofiber membrane with good morphology and mechanical properties by electrospinning, using tetraethyl orthosilicate (TEOS) and tetrabutyl orthotitanate (TBT) as silicon and titanium sources, and acetylacetone (AcAc) was used as an inhibitor of TBT hydrolysis. The effects of calcination temperature and TiO_2 content on the phase composition, microscopic morphology and strength of nanofiber membranes were studied, and the anti-infrared radiation mechanism of nanofiber membranes was analyzed. This research provides a certain experimental basis for the preparation of thermal protection systems suitable for different scenarios.

Experimental

Materials

Polyvinyl pyrrolidone (PVP, M_w = 10 000) was purchased from Tianjin Damao Chemical Reagent Co., Ltd., China. Tetraethyl orthosilicate (TEOS), oxalic acid ($H_2C_2O_4$), ethanol absolute and, *N*,*N*-dimethylformamide (DMF) and tetrabutyl titanate (TBT) were purchased from Tianjin Yongda Chemical Co., Ltd., China. Acetylacetone (AcAc) was purchased from Aladdin Chemical Reagent Co., Ltd., China. All chemicals were of analytical grade and used as received without further purification.

Sample preparation

Uniformly mix the TEOS and deionized water in a mass ratio of 1 : 1, and use oxalic acid as a catalyst. Solution A was obtained after 14 hours of magnetic stirring of the above mixture at room temperature. Fully mix 0.04 g, 0.08 g, 0.12 g and 0.16 g of TBT with 0.1 g AcAc and 0.5 g absolute ethanol respectively, and add the mixed solution of PVP and DMF to the above mixture, and then stir the mixture for 6 hours to obtain solution B. Under strong magnetic stirring, solution A was added dropwise to solution B to prepare a spinning precursor solution.

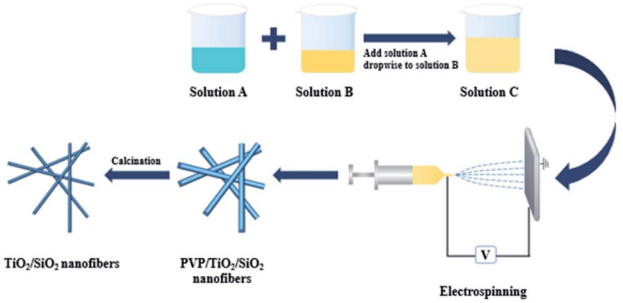

Scheme 1 Schematic diagram of the preparation process of SiO_2/TiO_2 composite fiber.

The PVP/SiO_2/TiO_2 precursor fiber membrane was prepared by a fully automatic electrospinning machine. Electrospinning parameters were as follows: at room temperature, the voltage was 15 kV; the needle was a 21G stainless steel needle, the distance between the needle and the receiving plate was 20 cm, and the precursor fluid flow rate was 0.1 mL h^{-1}.

The above PVP/SiO_2/TiO_2 precursor fiber membrane was dried and then put in a resistor furnace with smart temperature control, incinerated for 2 hours after the furnace temperature was increased to 600 °C, 800 °C, 900 °C and 1100 °C, respectively, at the rate of 2 °C min^{-1}, and then cooled to room temperature with the furnace (Scheme 1).

Characterization

The synthesis process of the sample was detected by thermal gravimetric analysis (TGA, SDT-Q600, TA, USA). The phase composition of the sample was detected by X-ray diffraction (XRD, XD6, Purkinje, China). The infrared spectrum of the sample was analyzed by Fourier transform infrared spectrometer (380, Nicolet, USA). The microscopic morphology of the sample was observed with a field emission scanning electron microscope (SEM, SU-8010, Hitachi, Japan). The thermal conductivity of the sample was measured with a thermal conductivity meter (TPS 2500S, Hot Disk, Sweden) using the transient planar heat source method. The tensile strength of the sample was analyzed using a tensile testing machine (INSTRON 5982, USA).

Results and discussion

Thermal decomposition process

In order to more intuitively demonstrate the mass loss and thermal effect of the sample during the calcination process, a precursor fiber membrane with a TiO_2 content of 16 wt% was selected for thermogravimetric analysis. The results are shown in Fig. 2. As can be seen from Fig. 1, the thermal decomposition process of the precursor fiber membrane can be roughly divided into four stages: the first stage is from room temperature to

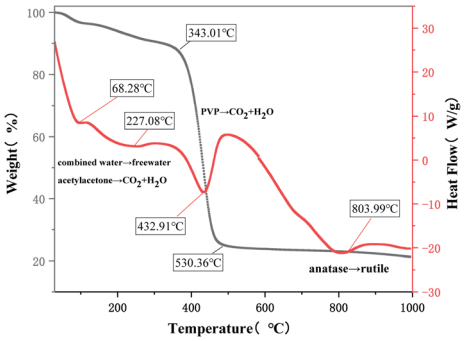

Fig. 1 DSC-TGA curves of the PVP/SiO_2/TiO_2 precursor fiber membrane (16 wt% TiO_2).

343.01 °C, the weight loss rate on the TGA curve was about 10.44%, corresponding to the obvious endothermic peaks at 68.28 °C and 227.08 °C on the DSC curve. The change in the first half of the TGA curve (from room temperature to 100 °C) at this stage was induced by the volatilization of free water and residual solvent adsorbed on the surface of the precursor fiber membrane. Changes in the second half (100–343.01 °C) were related to the loss of bound water, the decomposition of acetylacetone and PVP side chain. The second stage was when the temperature was between 343.01–530.36 °C. A large weightlessness step appeared on the TGA curve, with a weight loss rate of 61.99%, which corresponded to a large endothermic peak at 432.91 °C on the DSC curve. This is mainly caused by the carbonization of PVP and the complete decomposition of TEOS hydrolysate. When the temperature exceeded 530.36 °C, the TGA curve tended to be stable, and the weight loss rate basically did not change, indicating the completion of the thermal decomposition process of the precursor fiber membrane. The weight loss rate in the whole process was about 72%. The DSC curve showed an obvious endothermic peak at 803.99 °C, because the crystal structure of TiO_2 began to transform from anatase type to the stabler rutile type, which is an energy-absorbing process. Therefore, to prepare pure inorganic substances, the calcination temperature must be set to 530 °C and above. To obtain rutile TiO_2, the calcination temperature must be set to 803 °C and above.

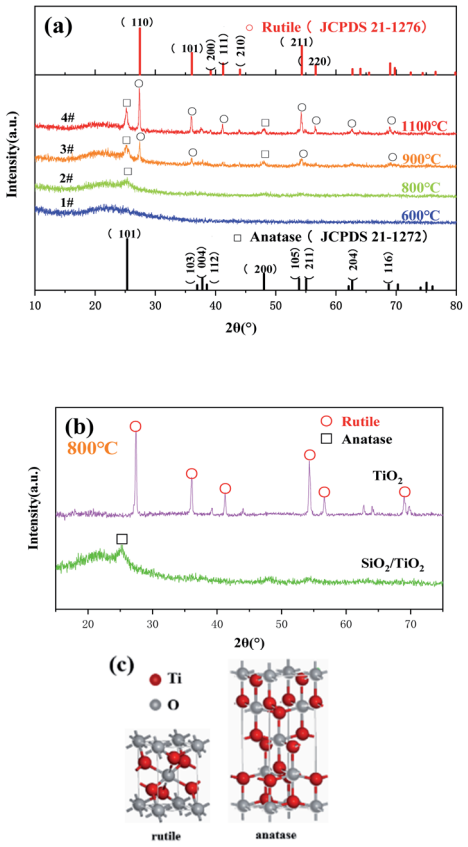

Fig. 2 (a) XRD patterns of SiO_2/TiO_2 composite fiber membranes calcined at different temperatures, (b) XRD patterns of TiO_2 and SiO_2/TiO_2 composite fiber membranes calcined at 800 °C, (c) lattice structures of rutile and anatase.

Phase and morphology analysis

In order to further clarify the phase composition of the samples at different calcination temperatures, XRD analysis was made on the products of the precursor fiber membranes calcined at different temperatures. Sample No. 1–4 are obtained by calcining the precursor fiber membrane (16 wt% TiO_2) from room temperature to 600 °C, 800 °C, 900 °C and 1100 °C at a rate of 2 °C min^{-1}. Fig. 2(a) shows the XRD patterns of four samples. As can be seen from it, a wide dispersion peak appeared in the four curves at $2\theta = 23°$, indicating that SiO_2 always exists in an amorphous state as the temperature increases. Diffraction curve of sample No. 1 had no other peaks except the amorphous diffraction peak of SiO_2, indicating that TiO_2 had not yet been crystallized at this temperature. After calcination at 800 °C, the curve had a low diffraction peak at $2\theta = 25.3°$ attributed to the anatase phase (101) crystal plane, indicating that TiO_2 had undergone a crystalline transformation at this temperature, but

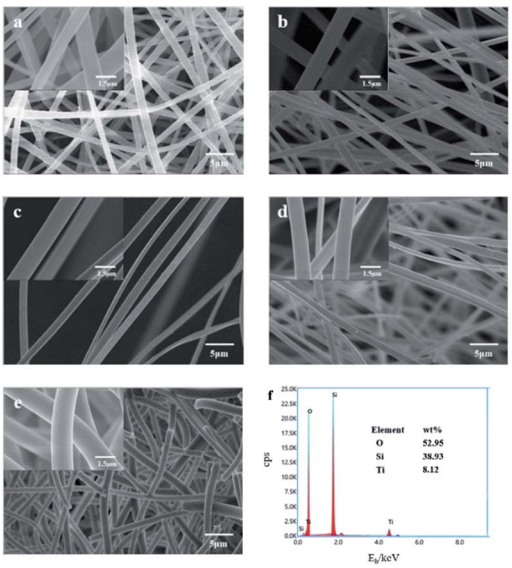

Fig. 3 (a–e) SEM images of precursor fiber membrane, sample No. 1, sample No. 2, sample No. 3 and sample No. 4; (f) energy spectrum of sample No. 3.

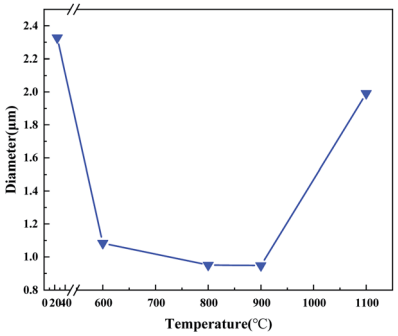

Fig. 4 The average diameter change curve of fiber membrane at room temperature and No. 1, No. 2, No. 3, and No. 4 samples.

the degree of crystallinity was low. As temperature rose, after calcination at 900 °C, sample No. 3 showed strong diffraction peaks on (101) and (110) crystal planes. Comparing the PDF cards JCPDS No. 21-1272 and JCPDS No. 21-1276, it is found that they belonged to the anatase-type and the rutile-type TiO_2. The degree of crystallization was further improved, and the crystal structure was gradually complete. It shows that the A-to-R crystal phase transition took place near this temperature range, which is consistent with the results of the DSC curve. The XRD curve of the product calcined at 1100 °C showed strong and sharp diffraction peaks on the crystal planes (101), (110), (111), (211) and (220), demonstrating that the crystal lattice of the product is complete and the crystal orientation is high. Seen from the changes of the four curves, as the calcination temperature increased, the SiO_2 in the product was always amorphous, and the TiO_2 changed from amorphous to anatase structure, and finally to rutile structure. According to Ostwald's step rule, during the growth and phase transition of a crystal, its metastable crystal form always appears first, and then changes to a stabler crystal form.[13] According to Pauling rule, the rutile structure has better stability than the anatase structure.[14] Therefore, as temperature rose, TiO_2 saw the change from amorphous to A and then to R. Fig. 2(b) shows the XRD patterns of precursor B calcined at 800 °C and sample No. 2. It can be clearly seen from the figure that the former is pure rutile TiO_2. Comparing it with Fig. 2(a), it can be seen that the crystallization degree of TiO_2 in SiO_2/TiO_2 composite fibers was significantly lower than that of pure TiO_2 fibers, indicating that the presence of SiO_2 had an inhibitory effect on the crystalline transformation of TiO_2. Possibly, in SiO_2/TiO_2 composite fibers, the volume-dominant SiO_2 phase closely surrounds the periphery of the TiO_2 lattice, and even cross-links with it, resulting in a lack of sufficient space in the TiO_2 lattice to achieve particle rearrangement. It has an inhibitory effect on its phase transition.[15]

Fig. 3(a)–(e) are the SEM images of the precursor fiber membrane and samples No. 1 to No. 4, and Fig. 3(f) is the energy spectrum of sample No. 3. Fig. 4 is a curve of the fiber diameter change of the precursor fiber membrane and its calcined product measured by Image J software. As can be seen from Fig. 3 and 4, the precursor fiber had a good morphology, good continuity, smooth surface and no adhesion. The products before and after calcination showed an irregularly-distributed three-dimensional network structure, and as the heat treatment temperature increased, the fiber diameter of the product decreased before increasing. The reason for this phenomenon can be explained as follows: after the precursor fiber was calcined at 600 °C, the product fiber diameter was greatly reduced due to the decomposition of the polymer template. However, there were still traces of organic components and voids left by the decomposition of the polymer template inside the fiber. After calcination at 800 °C and 900 °C, the remaining trace organic components were further removed, while the inorganic components collapsed, filling the voids inside the fiber and further reducing the diameter. After calcination at 1100 °C, the diameter of the fiber was greatly increased, and the breakage was increased, mainly because the high temperature destroyed the Si–O–Si covalent bond network structure in amorphous SiO_2. According to the EDS energy spectrum of sample No. 3, it can be determined that Ti element was present, and its content was 9.12%. This is consistent with the addition amount of each component in the preparation process of SiO_2/TiO_2 composite fiber. It shows that the electrospinning method can make SiO_2 and TiO_2 coexist stably in nanofibers.

Infrared analysis

Fig. 5 is the FTIR spectra of precursor A, precursor B and sample No. 3 under the same heat treatment conditions. As shown in the figure, peak at 1636 cm^{-1} is related to amide group and the one at 3420 cm^{-1} is related to hydroxyl. They are respectively related to the hydroxy (–OH) in the fiber bound water and free water.[16] It can be seen from Fig. 5(a) that the strong and broad absorption peaks in the range of 1000–1250 cm^{-1} and the absorption peaks near 798 cm^{-1} were attributed to the anti-symmetric and symmetrical stretching vibration peaks of Si–O–Si.[17] The product in Fig. 5(b) had a sharp absorption peak at 527 cm^{-1}, which corresponded to the characteristic peak of the Ti–O bond in TiO_2. This peak was red-shifted in Fig. 5(c), which can be explained as the presence of SiO_2 inhibits the phase transition of TiO_2, and there are more anatase TiO_2 with metastable structures in SiO_2/TiO_2 composite fibers.[18,19] This is consistent with the XRD analysis structure. Fig. 5(c) shows that the product had a characteristic vibration band of Ti–O bond in rutile TiO_2 near 427 cm^{-1}, again confirming that TiO_2 had

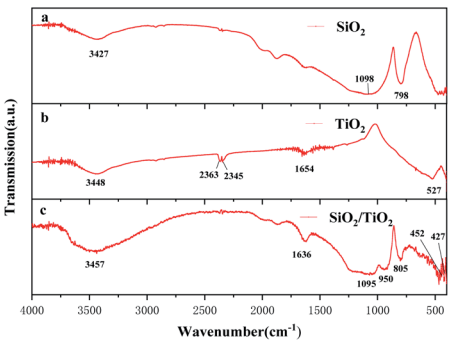

Fig. 5 FTIR spectra of SiO_2, TiO_2 and SiO_2/TiO_2 composite fibers calcined at 900 °C.

undergone a crystal phase transition at this temperature.[18] Compared with Fig. 5(a) and (b), Fig. 5(c) shows that the product had a new obvious absorption peak at 950 cm^{-1}. At present, there is no consensus on the attribution of the absorption peaks. Here we adopt the view of Zhai *et al.* and consider it to be the stretching vibration absorption peaks of Ti–OH and Ti–O–Si bonds,[20,21] indicating the occurrence of the bonding action of SiO_2 and TiO_2 in SiO_2/TiO_2 composite fibers.

Thermal radiation performance analysis

Under high temperature conditions, thermal radiation is the most important way of heat transfer between objects. Radiant thermal conductivity (k_r) reflects the ability of an object to conduct heat through thermal radiation, and can be calculated by the following formula:[22]

$$k_r = \frac{16 n_{total}^2 \sigma T^3}{3\beta_{total}} \quad (1)$$

In the formula, $\sigma = 5.67 \times 10^{-8}\ W\ m^{-2}\ K^{-4}$, which is the Stefan–Boltzmann constant; T is the thermodynamic temperature; n_{total} is the total refractive index of the composite material; β_{total} is the overall extinction coefficient. As can be seen from the formula, the extinction coefficient β is a key parameter that affects the attenuation ability of the material to light waves. Under normal circumstances, it can be obtained by Beer's law:[23]

$$\lg \frac{I_0}{I} = \beta c l \quad (2)$$

In this formula, I_0/I is the reciprocal of the infrared transmittance T; l is the optical path length; c is the concentration of the light-absorbing substance. Therefore, to compare the radiant thermal conductivity of different insulation materials, only the infrared transmittance of the material needs to be obtained.

Fig. 6 shows the infrared transmittance curves of fiber membranes with different TiO_2 content (0, 4%, 8%, 12% and 16%, respectively) after heat treatment at 900 °C in the range of 2.5–8 μm. It can be seen from the figure that under the same test conditions, as the content of TiO_2 increased, the infrared transmittance of the product continued to decrease, indicating that the addition of TiO_2 will significantly reduce the infrared transmittance of the fiber membrane. The infrared transmittance difference of the products ST-12 and ST-16 was small, indicating that when the content of TiO_2 sunscreen reaches a certain amount, increasing the content of TiO_2 produces no obvious effect on improving the radiant thermal conductivity of the nanofiber membrane.

Generally speaking, the infrared radiation incident on the material will be transmitted, reflected and absorbed. The mechanism of reflection of radiation on the surface of the material is very complicated, and it is not yet possible to get a satisfactory explanation from the perspective of quantum. From a macro point of view, the reflectivity R of the composite material can be obtained by the formula below:[24]

$$R = [(n_2 - n_1)/(n_2 + n_1)]^2 \quad (3)$$

In the formula, n_1 and n_2 are the refractive indices of the composite material when propagating in different media. According to formula (3), it is known that the composite material needs to have a high refractive index to achieve high reflectivity. Because of its dense structure, rutile TiO_2 has a higher refractive index than most other materials, and therefore a higher reflectivity.

The process of composite materials absorbing infrared radiation can be explained by the energy band theory. According to this theory, the band structure of semiconductor materials is composed of a valence band full of electrons and an empty conduction band. What is shown, basically, is that the titanium 3d, 4s, and 4p atonic orbitals are interacting with the oxygen 2s and 2p atomic orbitals to form a set of molecular orbitals having the usual bonding, antibonding, and nonbonding term symbols.[25] The top of the valence band is the unbonded Op_π orbital, and the bottom of the conduction band is the Tit_{2g} orbital. The energy interval between these two orbitals is called the forbidden band (E_g) of rutile TiO_2. When the incident infrared radiation reaches the band gap of rutile TiO_2, the electrons will absorb the energy and transit from the valence band to the conduction band, thereby absorbing fixed-frequency electromagnetic radiation.[26] In addition, TiO_2 particles can also convert the absorbed energy into infrasound waves, further weakening the intensity of infrared radiation in the original direction (Fig. 7).

Heat transfer process analysis

Fig. 8 shows the thermal conductivity curves at different temperatures of SiO_2 nanofiber membrane and SiO_2/TiO_2

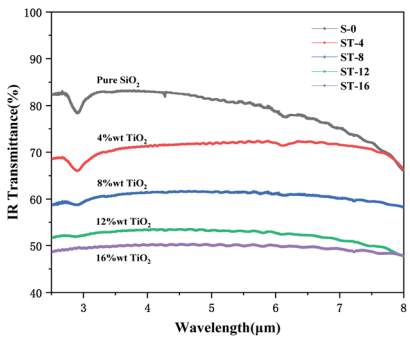

Fig. 6 Infrared transmittance curves of samples with different TiO_2 content.

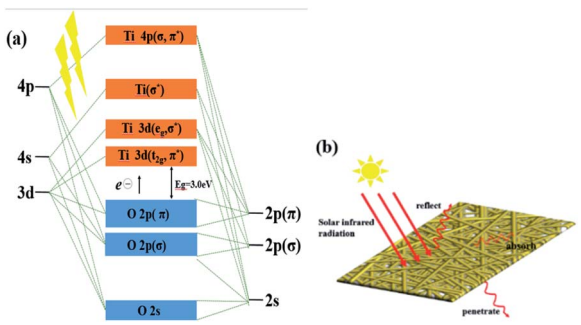

Fig. 7 (a) Energy band diagram of rutile TiO_2, (b) reflection, transmission and absorption of solar thermal radiation on the fiber membrane.

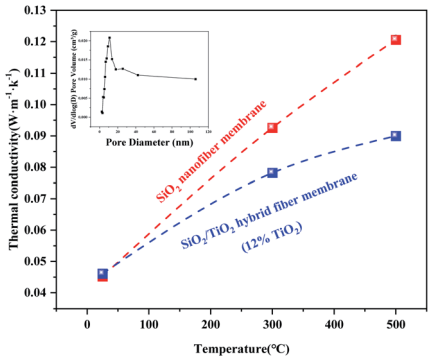

Fig. 8 The thermal conductivity change curves of the two fiber membranes at different temperatures and the BJH pore size distribution diagram of the composite fiber membrane.

composite fiber membrane (ST-12) after heat treatment at 900 °C. It can be seen from the figure that both fiber membranes had lower thermal conductivity at room temperature, being 0.045 W m^{-1} K^{-1} and 0.046 W m^{-1} K^{-1}, respectively, showing better thermal insulation performance than the common thermal insulation fiber felt in the market. As the test temperature going up, the thermal conductivity of the sample increases significantly. At 300 °C and 500 °C, the thermal conductivity of SiO_2 nanofiber membranes increased to 0.092 W m^{-1} K^{-1} and 0.12 W m^{-1} K^{-1}. After adding TiO_2, the thermal conductivity of the sample at these two temperatures decreased by 16% and 25%, respectively, to 0.078 W m^{-1} K^{-1} and 0.089 W m^{-1} K^{-1}. The properties of the composite fiber membrane and the existing high-temperature insulation materials are compared and the data are summarized in Table 1. It can be seen from the table that in the range of 400–600 °C, ST-12 has a lower thermal conductivity than most metal oxide fibers, and it is also in a reasonable range compared with pure SiO_2 fibers.

According to the BJH pore size distribution diagram, the product ST-12 is a typical mesoporous material, with the pore size mostly distributed between 10–30 nm, that is, much smaller than the mean free path of air.[27] Therefore, there was no gas thermal convection inside the fiber membrane, which is of great significance to improving its thermal insulation performance. Since the geometric scale of SiO_2 nanofibers is at the same magnitude as the mean free path of a particle of phonon, the scattering of phonons at the fiber boundary will greatly affect the energy transmission efficiency.[28] In addition, the nanoporous structure of the fiber membrane destroyed the connection network of solid SiO_2, and further reduced the solid-phase heat conduction of the material. When temperature rose, the thermal conductivity of the SiO_2 fiber membrane increased rapidly, while the thermal conductivity of ST-12 increased slowly. As the temperature increases, the proportion of radiant heat increases, and the shielding effect of TiO_2 on thermal radiation gradually appears, effectively reducing the thermal conductivity of the composite fiber membrane.

Fig. 9 shows the stress–strain curves of samples No. 1 to No. 3. It can be seen from the figure that as the calcination temperature changed, the initial modulus and tensile strength of the fiber membrane changed. The initial modulus of sample No. 1 was significantly smaller than that of sample No. 2 and sample No. 3, indicating that the fiber has better flexibility at 600 °C. Similarly, with the increase of the calcination temperature, the strength of the fiber membrane was also decreasing, being 3.6 MPa, 3.4 MPa and 3.09 MPa, respectively. This is because there were still a small number of organic components in the sample at 600 °C which would improve the toughness and strength of the fiber membrane. At high temperatures, the TiO_2 crystal lattice in the fiber was well developed, and the crystalline part destroyed the molecular chain in the amorphous region, resulting in a decrease in the strength of the fiber membrane. Even so, the strength of sample No. 3 can still meet its basic requirements as a thermal insulation material.

Conclusions

In summary, a flexible SiO_2/TiO_2 composite fiber membrane with good thermal insulation properties was prepared with the technology of electrospinning. The addition of TiO_2 with

Table 1 The comparative table on properties of high temperature insulation materials[2,24,29–31]

		Thermal insulation property			
Material	Tensile strength (MPa)	Thermal conductivity (W m^{-1} K^{-1})	Temperature difference on cold side (°C)	Test temperature (°C)	Test method
$CaZrO_3$ fibers		0.413		400	Laser flash method
SiO_2 fibers	3.2	0.12		500	Transient planar heat source method
ST-12	3.09	0.089		500	Transient planar heat source method
ZrO_2 fibers (plated with CeO_2–Y_2O_3 coating)		0.25		500	Laser flash method
ZrO_2 fibers (plated with TiO_2 coating)		0.6		600	Laser flash method
Y_2O_3 fibers	1.2		1124	1500	Temperature difference method

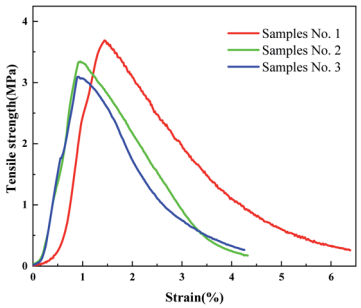

Fig. 9 Stress–strain curves of samples No. 1 to No. 3.

infrared shielding effect significantly reduced the thermal conductivity of the fiber membrane at high temperatures. And the cross-linking of SiO_2 and TiO_2 on the molecular scale ensured the good flexibility of the fiber membrane. In addition, after calcination at 900 °C, the composite fiber membrane with a TiO_2 content of 12% can achieve better overall performance at the lowest cost. In this scheme, the rutile TiO_2 had a higher conversion rate. The tensile strength of the sample was 3.09 MPa, and the thermal conductivity at 500 °C was 0.0899 W m^{-1} K^{-1}, which is 20% lower than that of pure SiO_2 fiber membrane. This kind of flexible thermal insulation material with excellent performance under high temperature conditions is expected to be fully applied in special occasions such as space suits and missile radomes.

Author contributions

Yilong Song: writing – original draft, formal analysis, resources and visualization; Fang Zhao: data curation and methodology; Zhizun Li: project administration and supervision; Zhaogang Cheng: funding acquisition; Hongjun Huang: conceptualization; Mifen Yang: writing – review & editing.

Conflicts of interest

There are no conflicts to declare.

Acknowledgements

This work is supported by the Hebei Natural Science Foundation of China (E2015506011) and Innovation and Development Science Foundation of the PLA Army Engineering University Shijiazhuang Campus (KYSZJQZL1910).

Notes and references

1 B. Eggertsson Dagur, *Lancet Planet. Health*, 2021, **5**(2), e71.
2 Y. S. Si, X. Mao, H. X. Zheng, J. Y. Yu and B. Ding, *RSC Adv.*, 2014, **5**(8), 6027–6032.
3 Y. Liu, D. Pan, W. Chen, W. Q. Wang, H. Shen and H. X. Xu, *Acta Phys. Sin.*, 2020, **69**(03), 7–24.
4 H. Brendel, G. Seifert and F. Raether, *J. Thermophys. Heat Transfer*, 2017, **31**(2), 463–472.
5 X. S. Zhang, B. Wang, N. Wu, C. Y. Wu and Y. D. Wang, *J. Inorg. Mater.*, 2021, **36**(03), 245–256.
6 H. X. Zhang, X. D. He and F. He, *J. Alloys Compd.*, 2009, **469**(1–2), 366–369.
7 J. Yang, H. Wu, M. Wang and Y. Liang, *Int. J. Heat Mass Transfer*, 2018, **117**, 729–739.
8 D. H. Ma, L. Y. Zhu and B. L. Liu, *Ceram. Int.*, 2020, **46**(3), 3400–3405.
9 Y. Yu, Y. Zhao, Y. L. Qiao, Y. Feng and W. D. Fei, *J. Mater. Sci. Technol.*, 2021, **84**, 10–15.
10 W. E. Grunert and F. Notaro, *AIAA 4th Thermophysics Conference*, 1969, pp. 40–45.
11 D. M. Anderson, J. R. Fessler, M. A. Pooley, S. Seidel and J. F. Brennan, *Biomed. Opt. Express*, 2017, **8**(3), 1698.
12 D. Q. Zhao and F. Yang, *Infrared Technology*, 2002(05), pp. 57–59.
13 G. T. Rengarajan, D. Enke, M. Steinhart and M. Beiner, *Phys. Chem. Chem. Phys.*, 2011, **13**(48), 21367–21374.
14 P. Huang, B. Shang, L. J. Li and J. L. Lei, *Chin. J. Chem. Phys.*, 2015, **28**(6), 681–687.
15 R. D. Shannon, *J. Appl. Phys.*, 1964, **35**(11), 3414–3416.
16 Q. Chen, J. Dong, W. Shi, W. Dong and X. Yao, *Appl. Surf. Sci.*, 2009, **255**(18), 7918–7924.
17 W. S. Xiao, W. S. Peng, G. X. Wang, F. Y. Wang and K. N. Weng, *Spectrosc. Spectral Anal.*, 2004, **24**(6), 690–693.
18 L. S. Yin, H. Shen and J. X. Zhang, *Acta Electron.*, 2002, (06), 808–810.
19 L. P. Sun, S. Gao, H. Zhao, L. H. Huo and J. G. Zhao, *Journal of Light Scattering*, 2003, (04), 300–302.
20 J. W. Zhai, L. Y. Zhang and X. Yao, *J. Funct. Mater.*, 1997, (05), 46–47.
21 L. Zhao, D. X. Wang, J. S. Gao and C. M. Xu, *Chin. J. Catal.*, 2005, (01), 15–19.
22 J. Kuhn, T. Gleissner, M. C. Arduini-Schuster, S. Korder and J. Fricke, *J. Non-Cryst. Solids*, 1995, **186**, 291–295.
23 L. Bai and Y. T. Xin, *Electro-Optic Warfare & Radar Passive Countermeasures*, 2002(03), pp. 17–18.
24 X. Z. Gan, PhD thesis, Shandong University, 2018.
25 W. D. Fischer, *Phys. Rev. B: Solid State*, 1972, **5**(11), 4219–4226.
26 F. M. Hossain, A. V. Evt, I. V. Belova, J. Nowotny and G. E. Murch, *Comput. Mater. Sci.*, 2010, **48**(4), 854–858.
27 X. Lu, M. C. Arduini-Schuster, J. Kuhn, O. Nilsson, J. Fricke and R. W. Pekala, *Science*, 1992, **255**(5047), 971–972.
28 W. Y. Chen, PhD thesis, Southeast University, 2017.
29 S. Y. Shi, K. K. Yuan, C. H. Xu, X. T. Jin, Y. S. Xie, Z. H. Wang, X. Q. Wang, L. Y. Zhu, G. H. Zhang and D. Xu, *Ceram. Int.*, 2018, S0272884218311283.
30 J. M. Yang, H. J. Wu, M. R. Wang and Y. Y. Liang, *Int. J. Heat Mass Transfer*, 2018, **117**, 729–739.
31 Y. S. Xie, L. Wang, B. X. Liu, L. Y. Zhu, S. Y. Shi and X. Q. Wang, *Mater. Des.*, 2018, **160**(DEC), 918–925.